Current Research (2026) Newfoundland and Labrador Department of Energy and Mines Geological Survey, Report 26-1, pages 63-81

STRUCTURAL COMPLEXITY IN THE VOLCANIC BULL ARM FORMATION, SOUTHEASTERN ISTHMUS OF AVALON, NEWFOUNDLAND, AS REVEALED BY UAV PHOTOGRAMMETRY, STRUCTURAL FIELD DATA AND LINEAMENT ANALYSIS

A.J. Mills and Z.V. Adam
Regional Geology Section

ABSTRACT

Unmanned aerial vehicle (UAV) photogrammetry was conducted along a 350-m coastline section at Bellevue Beach, southeastern Isthmus of Avalon to generate a high-resolution basemap for draping and analysing geological field observations. To support regional structural interpretation, a lineament dataset was created for the Isthmus of Avalon and adjacent areas, using Landsat imagery, Digital Elevation Models (DEM) and bathymetric data. Lineament analysis defines a regional, post-Cambrian structural pattern interpreted to reflect sinistral strike-slip displacement (D_2) along a north-trending fault or principal shear zone located near the Spread Eagle Thrust. In the isthmus area, sinistral displacement apparently involved the rotation of pre-existing, east- and northeast-trending D_1 structures into near-parallelism with the north-trending Spread Eagle Thrust, and may have accompanied coeval, antithetic, extensional structures, now represented by short (~4–5 km), northwest-trending lineaments. Sinistral strike-slip deformation elsewhere has been linked to the accretion of Avalonian terranes to the composite Laurentian margin during the Acadian Orogeny, commonly including re-activation of older structures.

Along the Bellevue Beach section, primary contacts and stratigraphy are locally difficult to resolve because of a lack of younging up indicators and the presence of abundant faults, some of which form conjugate sets. Thrust faults, observed at one location, indicate an early, southeast-directed thrust imbrication, possibly related to the late Ediacaran Avalonian orogeny (D_1). Progressive deformation is inferred to have steepened originally low-angle faults, and locally overturned bedding and folds. A subsequent east–west shortening event, interpreted to be related to Acadian (or later) orogenesis (D_{3a}), is associated with south-southwest- and north-northeast-plunging fold axes and the regionally developed penetrative axial planar cleavage. Quartz-filled tension gashes likely formed late during this east–west compressional event (D_{3b}) and indicate subvertical extension possibly related to orogenic collapse. These structures are truncated by a set of conjugate subvertical faults that formed under either northeast–southwest transpression or northwest–southeast extension possibly during assembly or breakup of Pangea (D_4), respectively. Further detailed structural investigations, stratigraphic studies, geochronology and expanded lineament analysis are recommended to refine these interpretations.

INTRODUCTION

The Isthmus of Avalon is the narrow landmass that connects the Avalon Peninsula to the main part of the island of Newfoundland (Figure 1). Considered part of the central Avalon Zone (*sensu* Myrow, 1995), the region is underlain mainly by Ediacaran rocks of the marine turbiditic Connecting Point Group to the west and the unconformably overlying volcano-sedimentary Musgravetown Group to the east. Previous geological mapping in the area includes Geological Survey of Canada bedrock mapping at a scale of one inch to one mile (McCartney, 1957, 1958), unpublished theses (Malpas, 1971; Mills, 1991), and regional bedrock geology compilations (McCartney, 1967; King, 1988). No detailed structural investigations have been documented for this area. The Mineral Occurrence Data System (https://gis.gov.nl.ca/mods) indicates that commodities of economic interest identified in the area include lead, barite and copper. Most of the mineral showings are vein-hosted and have not been actively exploited since the 1800s and early 1900s (Howse and Maloney, 1984). This study focuses on structural features in the Bellevue Beach area, southeastern Isthmus of Avalon, and surrounding areas.

The use of unmanned aerial vehicle (UAV) photogrammetry has become increasingly popular in geological investigations, as it provides high-resolution imagery that can serve as a basemap on which to overlay detailed field obser-

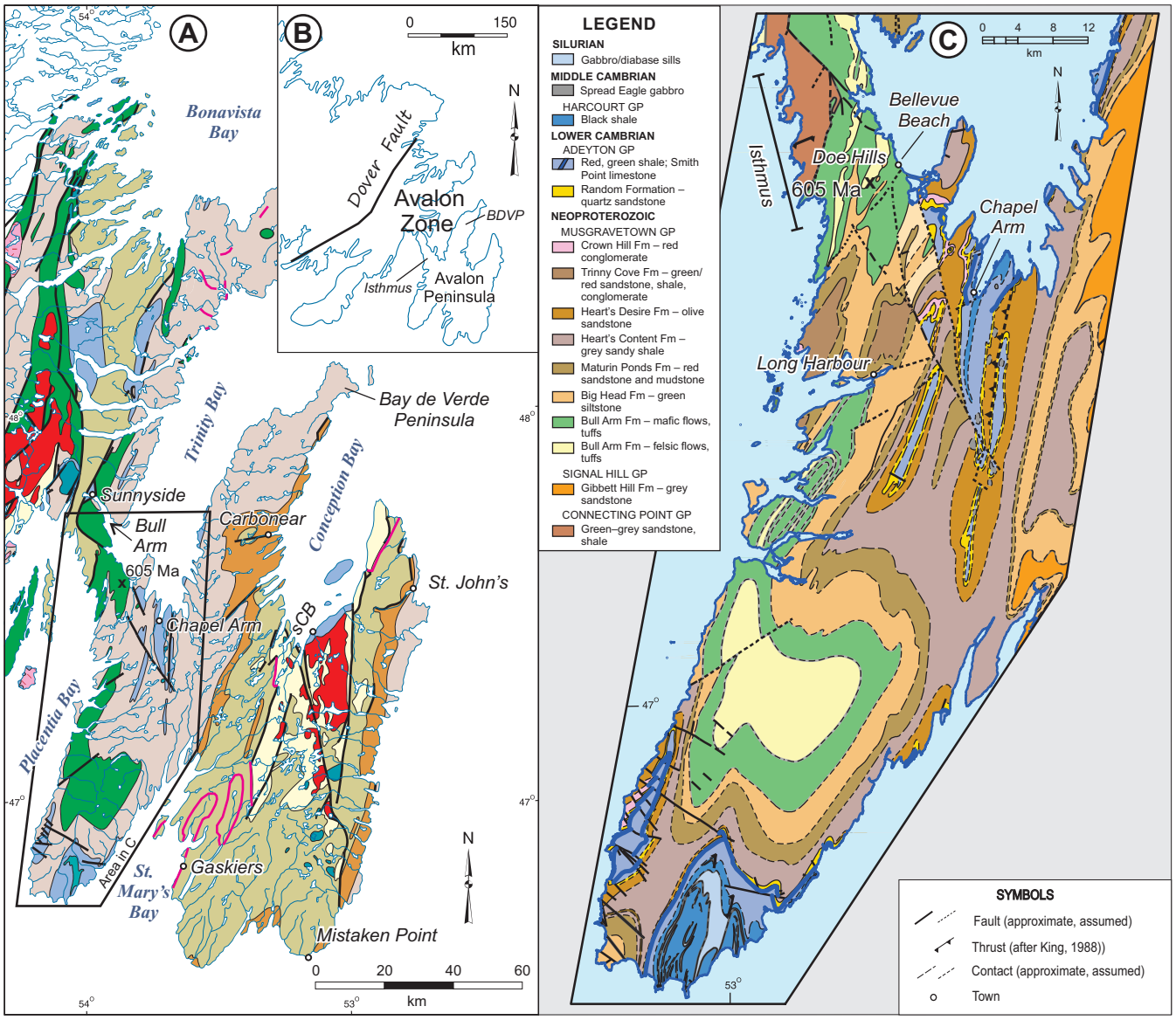

LEGEND

DEVONIAN AND CARBONIFEROUS INTRUSIVE ROCKS
- Mainly granites; posttectonic relative to latest formation

NEOPROTEROZOIC TO EARLY ORDOVICIAN STRATIFIED ROCKS
- Shallow-marine, mainly fine-grained, siliciclastic rocks, including minor limestone and volcanic rocks

NEOPROTEROZOIC
- Fluviatile and shallow-marine siliciclastic rocks (Signal Hill Group, upper Musgravetorn Group)
- Marine deltaic siliciclastic rocks (St. John's Group)
- Marine turbidites (Conception and Connecting Point groups)
- Gaskiers Formation, Trinity facies (glacial diamictite, Conception and Musgravetown groups)
- Mainly subaerial volcanic rocks (lower Musgravetown Group)
- Submarine to subaerial volcanic rocks (Harbour Main Group)

NEOPROTEROZOIC TO CAMBRIAN INSTRUSIVE ROCKS
- Mafic intrusions
- Granitoid intrusions, including unseparated mafic phases

SYMBOLS
- Geological contact, fault
- Town, U–Pb (zircon) age

Figure 1. *A) Bedrock geology map for the eastern Avalon Zone in Newfoundland (modified from Colman-Sadd* et al.*, 1990); B) Inset map showing the Avalon Zone in Newfoundland; C) Bedrock geology map for the western Avalon Peninsula and the Isthmus of Avalon (after King, 1988); fold traces are omitted for clarity. BDVP–Bay de Verde Peninsula, sCB–southern Conception Bay.*

vations and data, thereby augmenting outcrop analysis. Applications of such imagery include outcrop characterization (*e.g.*, Chesley *et al.*, 2017), sedimentary and basin analysis (*e.g.*, Bilmes *et al.*, 2019), fracture analysis (*e.g.*, Menegoni *et al.*, 2018; Peace and Jess, 2022), geomorphological analysis (*e.g.*, Lazzari and Gioia, 2017), and resource assessment and delineation (*e.g.*, Jackisch *et al.*, 2020). Here, we employ a conventional workflow to collect drone imagery from an underexplored, but exceptionally exposed coastal section on the southern Isthmus of Avalon to serve as a basemap for field-based observations. We then combine our results with regional lineament analysis to gain a more regional perspective and insight into the deformation and structural evolution of this poorly understood part of Newfoundland's Avalon Zone.

The purpose of this study is five-fold: 1) to obtain high-resolution drone imagery as a basemap for the current and future detailed geological investigations; 2) to explore the efficacy of lineament analysis as a method to provide insight into the structural evolution of the central Avalon Zone; 3) to highlight some of the structural features exposed along the coastal bedrock section at Bellevue Beach; 4) to illustrate the previously understated structural complexity of the Avalon Zone in Newfoundland; and 5) to recommend avenues for future research in this (and other) well exposed and easily accessed part(s) of the Avalon Zone.

REGIONAL GEOLOGY

The Avalon Zone (Avalonia), the most eastern lithotectonic domain in Newfoundland, extends westward to the Dover Fault (Blackwood and Kennedy, 1975), which separates it from the Gander Zone (Ganderia) to the west. The central part of Newfoundland's Avalon Zone is underlain by upper Ediacaran rocks of the Connecting Point Group and the unconformably overlying Musgravetown Group (Figure 1). The Connecting Point Group comprises mainly deep-marine turbiditic strata, whereas the Musgravetown Group, to the east, comprises a lower bimodal volcanic sequence conformably overlain by shallow-marine to terrestrial sedimentary rocks. The contact between these two units is nearly everywhere faulted but is preserved as an unconformity at several localities in the western Bonavista Bay area (Hayes, 1948; Jenness, 1963; Mills, 2014). In Bonavista Bay, ~95 km north of the current study area, deformed *ca.* 605 Ma lithic tuff of the upper Connecting Point Group is unconformably overlain by *ca.* 600 Ma crystal tuff of the lowermost Musgravetown Group, thus constraining deformation of the older strata to a 5 m.y. period that marks a depositional gap between the groups (Mills *et al.*, 2016b). Less than 4 km to the southwest of Bellevue Beach, the Doe Hills rhyolite (Figure 1C) yielded a U–Pb (zircon) crystallization age of *ca.* 605 Ma (Mills *et al.*, 2017) for the Bull Arm Formation, the lowermost stratigraphic unit of the Musgravetown Group (McCartney, 1967; King, 1988) in the isthmus area.

All rocks within the Bellevue Beach area are part of the Bull Arm Formation, which includes mafic and felsic flows as well as voluminous pyroclastic and lesser clastic sedimentary rocks. The Bull Arm Formation is regionally overlain to the south and east by mainly green siltstone and sandstone of the Big Head Formation, itself overlain by the heterolithic Maturin Ponds and Trinny Cove formations (McCartney, 1967; King, 1988). At Long Harbour, 24 km south of Bellevue Beach, the Big Head Formation contains a distinctive diamictite unit that is likely correlative to glacially derived deposits of the Gaskiers Glaciation (Brückner, 1977; Mills and Sandeman, 2021). Deep- and shallow-marine glacial deposits of the coeval *ca.* 580 Ma Gaskiers Formation and Trinity Diamictite, occur on the Avalon and Bonavista peninsulas, respectively (Pu *et al.*, 2016; Fitzgerald *et al.*, 2024; Gómez *et al.*, 2025). All rock types exposed along the Bellevue Beach section were likely deposited between *ca.* 605 and 580 Ma.

The deformation history of the eastern and central parts of Newfoundland's Avalon Zone remains poorly understood, with no published detailed structural studies and limited unpublished works including field trip guidebooks (*e.g.*, Calon, 2001), theses (*e.g.*, Rice, 1996; Riveros, 1998; Peddle, 2017; Calon, 2017) and government reports (*e.g.*, Mills *et al.*, 2016a; Mills and Jones, 2024). In the northwestern Avalon Zone, the Dover Fault initiated as a ~20-km-wide shear zone that records *ca.* 422–394 Ma sinistral-oblique Acadian accretion of Avalonia to the composite Laurentian margin (Caron, 1994; Holdsworth, 1994; D'Lemos *et al.*, 1997; Kellett *et al.*, 2016). Sinistral strike-slip elsewhere in the Appalachians has also been linked to accretion of Avalonian terranes to the composite Laurentian margin during the Acadian Orogeny (Waldron *et al.*, 2022), commonly reactivating older structures. Subsequent reactivation in northwestern Avalon Zone was focused along narrower, dextral deformation zones associated with limited displacement (Holdsworth, 1994) and likely developed by *ca.* 385 Ma (Kellett *et al.*, 2016).

Miller and Singh (1995) combined existing onshore and offshore geophysical data to better understand the structural history of the Avalon Zone and suggested that the dominant arcuate, north-trending patterns reflect the oldest (Precambrian) structural features. Riveros (1998) conducted structural investigations around southern Conception Bay (sCB; Figure 1), where a sub-Cambrian unconformity facilitated the distinction between Precambrian and post-Cambrian structural elements. Some north- and northeast-trending faults in the sCB area were concluded to be

Precambrian by virtue of being truncated by the sub-Cambrian unconformity. Riveros (1998) suggested that the approximately north-trending faults are the oldest structural elements and typically occur as normal faults that have undergone reactivation. Four deformation events were constrained by their relative timing with respect to the sub-Cambrian unconformity and to each other (Riveros, 1998). The first event, D_{1a}, was a Precambrian block-faulting extensional event that produced north-trending faults that separated horsts and grabens in the sCB area. The second event, D_{1b}, involved north–south shortening associated with northwest-trending dextral and northeast-trending sinistral kink bands. A S_1 cleavage was locally identified near tight to isoclinal F_1 folds but is regionally non-penetrative. The trace of these Precambrian structures is truncated by the sub-Cambrian unconformity and attributed to the Ediacaran Avalonian orogeny (*e.g.*, Beranek *et al.*, 2023; Serna Ortiz and Lowe, 2024). The regionally developed and pervasive cleavage, S_2, is associated mainly with north-northeast-trending folds and reflects east–west shortening during D_{2a}. These post-Cambrian structural features dominate the regional map pattern and are considered elements of the main compressional deformation event, likely related to the mid-Paleozoic Acadian Orogen (*e.g.*, Anderson *et al.*, 1975; Calon, 2001). An extensional D_{2b} event involved reactivation of pre-existing faults (all generations) in an overall northwest–southeast oriented extensional regime.

METHODS

Aerial photogrammetry was performed in a single DJI Air 3 manually piloted flight survey at 15:00 on May 29, 2025, along the east-facing wall of Bellevue Beach. Agisoft Metashape was used to process the photography and generate point clouds, meshes and orthorectified photomosaics (orthomosaics). 109 geotagged aerial photographs were captured across two flight paths along the coastal section: one path with a wide-angle 24 mm camera and another with a telephoto 70 mm camera to provide full coverage. Photographs were aligned using the built-in GPS of the DJI Air 3. A dense point cloud was constructed from depth maps, overlain by a textured mesh surface built from the dense point cloud and aerial images. An orthomosaic was built from the mesh model using a mosaic blending mode and custom planar projection to capture the vertical surface.

Lineament extraction was completed in ArcGIS Pro using bathymetric data, digital elevation models (DEM) and Landsat 8 multispectral data. Landsat images were processed in ENVI 6.1. All lineaments were manually extracted from filtered images using edge enhancement and detection techniques (Ahmadi and Pekkan, 2021). Bathymetry data acquired along the Bull Arm inlet at 100-m spacing were retrieved from the CHS NONNA Data Portal (https://data.chs-shc.ca/login). An Empirical Bayesian Kriging Regression analysis was used on these measurement points to create a bathymetry prediction surface, which was then followed by a slope analysis to highlight steep features. The DEM image was first sharpened with a Gaussian high-pass filter followed by a Laplacian filter, viewed in parallel with a multidirectional hillshade. Multispectral Landsat 8 scenes were acquired August 30, 2024, at 14:23 UTC, with a solar azimuth of 152° and land cloud cover of 10%. Principal component analysis (PCA) revealed that the first principal component (PC1) contained 98% of the variance. A Gaussian low-pass filter was applied to PC1 for data smoothing and noise reduction followed by directional filtering of east–west, north–south, northeast and northwest directions.

Strike and dip measurements were collected using a Brunton compass and planar features are reported using the right-hand-rule convention. The magnetic declination at Bellevue Beach was 17°W in August of 2025. Locations were plotted on the drone-generated imagery using both geotagged photographs acquired by a GPS-enabled Nikon COOLPIX W300 camera, and by visual positioning estimates. Stereonet 11 software (*see* Allmendinger *et al.*, 2013) was utilized to project primary and deformation structures on equal-area stereonets. The coastal section is best accessed from the south, at the day-use area for Bellevue Beach Campground. Northern parts of the section are only accessible at low tide.

RESULTS

PHOTOGRAMMETRY

Detailed digital imagery and structural measurements were acquired over approximately 350-m length of coastal exposure at Bellevue Beach (Appendix 1). The resulting orthomosaic has a resolution of 7.12 mm/px and is available for download in Geofiles (https://gis.gov.nl.ca/ minesen/ geofiles/default.asp). The drone imagery is displayed in Figure 2, where it is annotated and subdivided into four panels for clarity.

LINEAMENT ANALYSIS

Observational analysis of the lineament trends (Figure 3) allowed the distinction of four principal orientations, with considerable overlap: a north–south trending set (Spread Eagle), a northwest trending set (Bull Arm), a northeast trending set (Bay de Verde), and an east–west trending set (Carbonear), the latter occurring predominantly closer to Conception Bay.

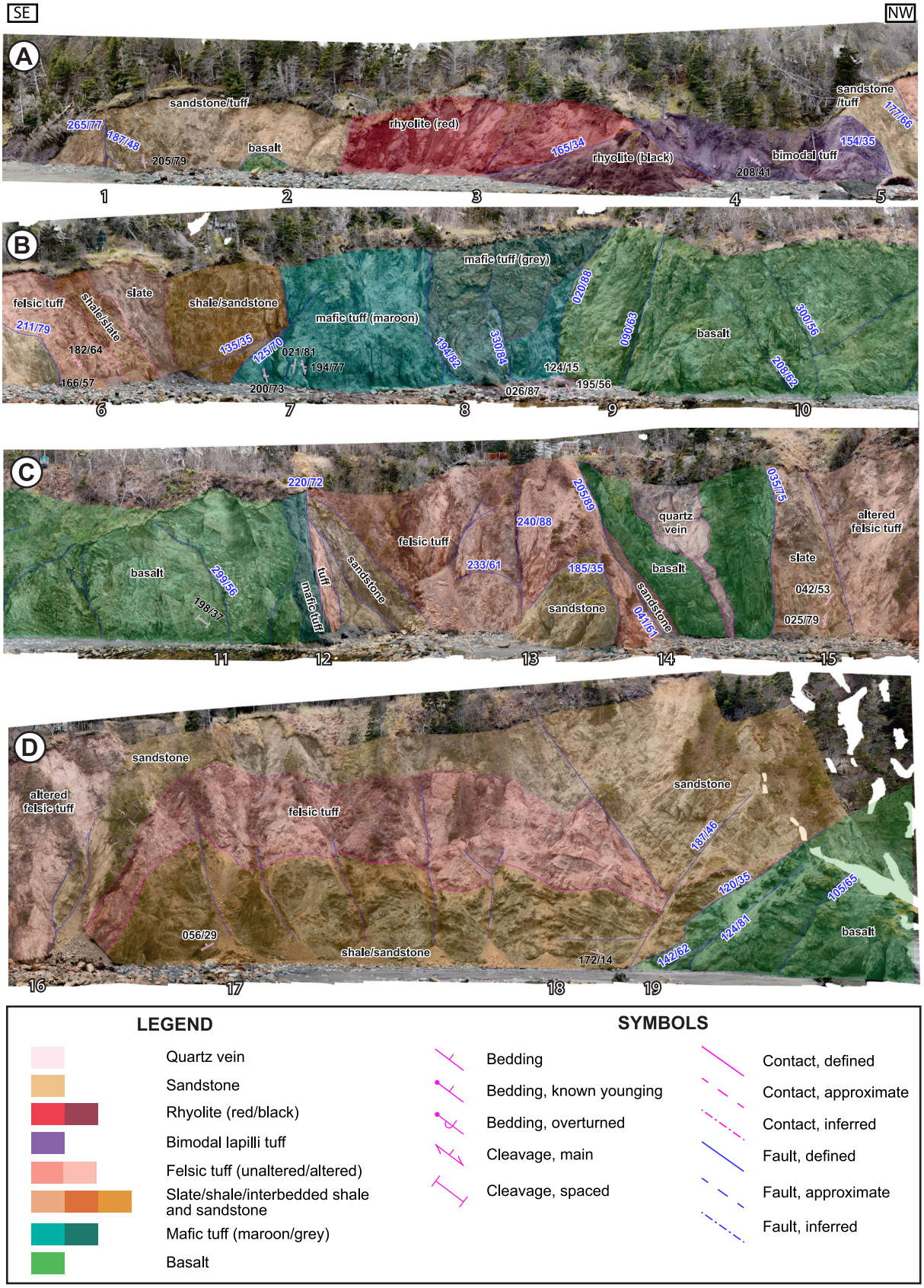

Figure 2. *Orthomosaic of coastal exposure along Bellevue Beach, overlain with mapped faults and geological interpretation, divided into 4 panels moving from southeast to northwest. Stations are indicated at the bottom of each panel.*

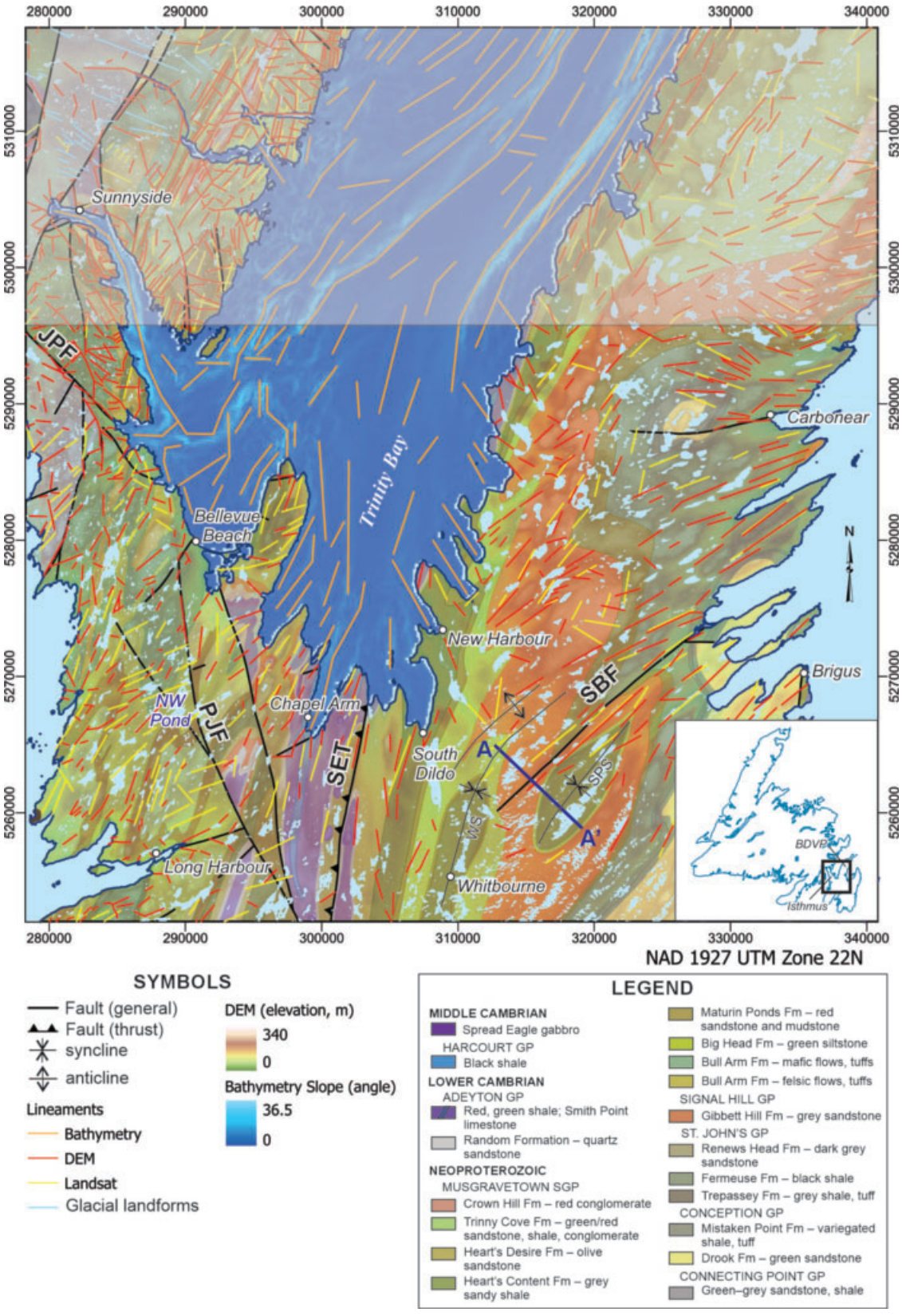

Figure 3. *Results of lineament analysis covering part of the north-central Avalon Zone (*see *inset). Lineaments beneath the grey transparent box were omitted from analysis. Bedrock geology after King (1988). BDVP–Bay de Verde Peninsula, JPF–Jacks Pond Fault, PJF–Placentia Junction Fault, SBF–Shearstown Brook Fault, SET–Spread Eagle Thrust, SPS–Snows Pond syncline, WS–Whitbourne syncline.*

Table 1 shows the distribution of lineaments grouped by source (DEM, bathymetry or Landsat imagery). While the data are heavily influenced by the DEM, producing both the highest number of lineaments (73.32% of the total) and the greatest total length (58.81% of the total), the lineaments extracted from the bathymetry data have a greater mean length (2635.32 m) than those from the DEM (1148.07 m), while representing only 7.39% of the total lineaments. Lineaments extracted from the Landsat imagery reflect similar proportions of the total number (19.29%) and total length (27.59%) of lineaments.

Table 1. Distribution of lineaments grouped by data source (DEM, bathymetry, Landsat)

Source	Count	% of total count	Total length per source (m)	Mean length (m)	% of total length
DEM	665	73.32	763470	1148.07	58.81
Bathymetry	67	7.39	176567	2635.32	13.60
Landsat	175	19.29	358264	2047.22	27.59
Total	907	100	1298300	5830.62	100

To account for the uneven distribution of lineament length, the lineaments were weighted by their individual line length. Normalized line length was calculated by dividing the length of each lineament by the total summed lengths of all lineaments, which was then aggregated by trend. Table 2 shows the summarized results of the length-corrected data within each trend bin and Table 3 shows the relative proportion of each lineament set (by orientation) as determined by each source.

Lineaments from the DEM and Landsat datasets with a west-northwest-trend in the area north of Sunnyside were initially deemed suspect based on their nearly orthogonal trend relative to trends that reflect bedrock features on existing bedrock maps (*e.g.*, King, 1988). They were therefore critically examined by J. Organ and H. Campbell (pers. comm., 2025), compared to known surficial landform trends (McHenry and Dunlop, 2016; Norris *et al.*, 2024) and interpreted to represent glacial landforms. Accordingly, west-northwest-trending lineaments determined to reflect surficial processes rather than tectonic ones were then excluded from the structural analysis. Further culling of lineaments from the dataset excluded all lineaments in the northern part of the study area (grey transparent box; Figure 3) to reduce the high number of northeast-trending lineaments that would otherwise artificially dilute the relative proportion of the other lineament trends.

The Spread Eagle and Carbonear trends are most apparent in the DEM- and bathymetry-based lineaments (Figure 4B, C). The Bull Arm trend is most apparent in the bathymetry-derived lineaments (Figure 4C). The Bay de Verde trend is the dominant orientation in all three data sources (Figure 4A–D).

FIELD OBSERVATIONS

Structural data were collected along the section coincident with aerial photogrammetry (*see* below). All field data are compiled in a summary table given in Appendix 2.

Rock types encountered along the Bellevue Beach section include massive to amygdaloidal basalt, black and red rhyolites, mafic lapilli tuff, felsic and bimodal lithic tuffs, maroon and green shales (locally slates), and dark-grey and buff- to pale-grey sandstones. The stratigraphy of the section is characterized by predominantly subvertical bedding, with commonly equivocal top indicators and abundant faulted contacts. Figure 2 conveys the interpreted stratigraphic relationships along the Bellevue Beach section.

Bedding

Bedding orientations along the section range from shallow to steep and overturned. Local younging directions were determined mainly within the sedimentary rocks intercalated with the dominantly volcanic and pyroclastic units. In

Table 2. Summarized lineament distribution within each trend bin (N, NW, NE, E), corrected for line length

Group (azimuth)	Count	% of total count	Total length per group (m)	% Total length	Mean length (m)	Normalized by source (%)
N (0–25)	141	15.55	241274	18.58	1711.16	22.16
NW (140–165)	61	6.73	82565	6.36	1353.53	8.71
NE (25–50)	273	30.10	387933	29.88	1421.00	30.39
E (80–105)	106	11.69	103419	7.97	975.65	6.19
Other	326	35.94	483109	37.21	1481.93	32.55
Total	907	100	1298300	100	6943.27	100

Table 3. Distribution of lineaments by source (DEM, bathymetry, Landsat) within trend bin (N, NW, NE, E)

Source	DEM		Bathymetry		Landsat	
Group	n	%	n	%	n	%
N	83	12.48	17	25.37	41	23.43
NW	46	6.92	11	16.42	4	2.29
NE	188	28.27	25	37.31	60	34.29
E	98	14.74	5	7.46	3	1.71
Other	250	37.59	9	13.43	67	38.29
Total	665	100	67	100	175	100

those latter units, flow tops are rarely discernible. At the south end of the section (Figure 2A), bedding is steeply west-dipping and overturned (east-younging). Primary layering is absent in the red and black rhyolites and bimodal tuffs along most of the first panel of the section. Normal grading in mafic lithic tuff at Station 7 (Figure 2B) indicates that the steeply north-northwest-dipping beds are overturned. Near the north end of the mafic tuff unit (Station 9), a south-southwest-plunging asymmetric cylindrical anticline has a steeply dipping southeastern limb and a gently dipping northwestern limb (Plate 1). Much of the section to the northwest includes basaltic flows and tuffs that do not preserve primary layering. Steeply bedded pyroclastic rocks

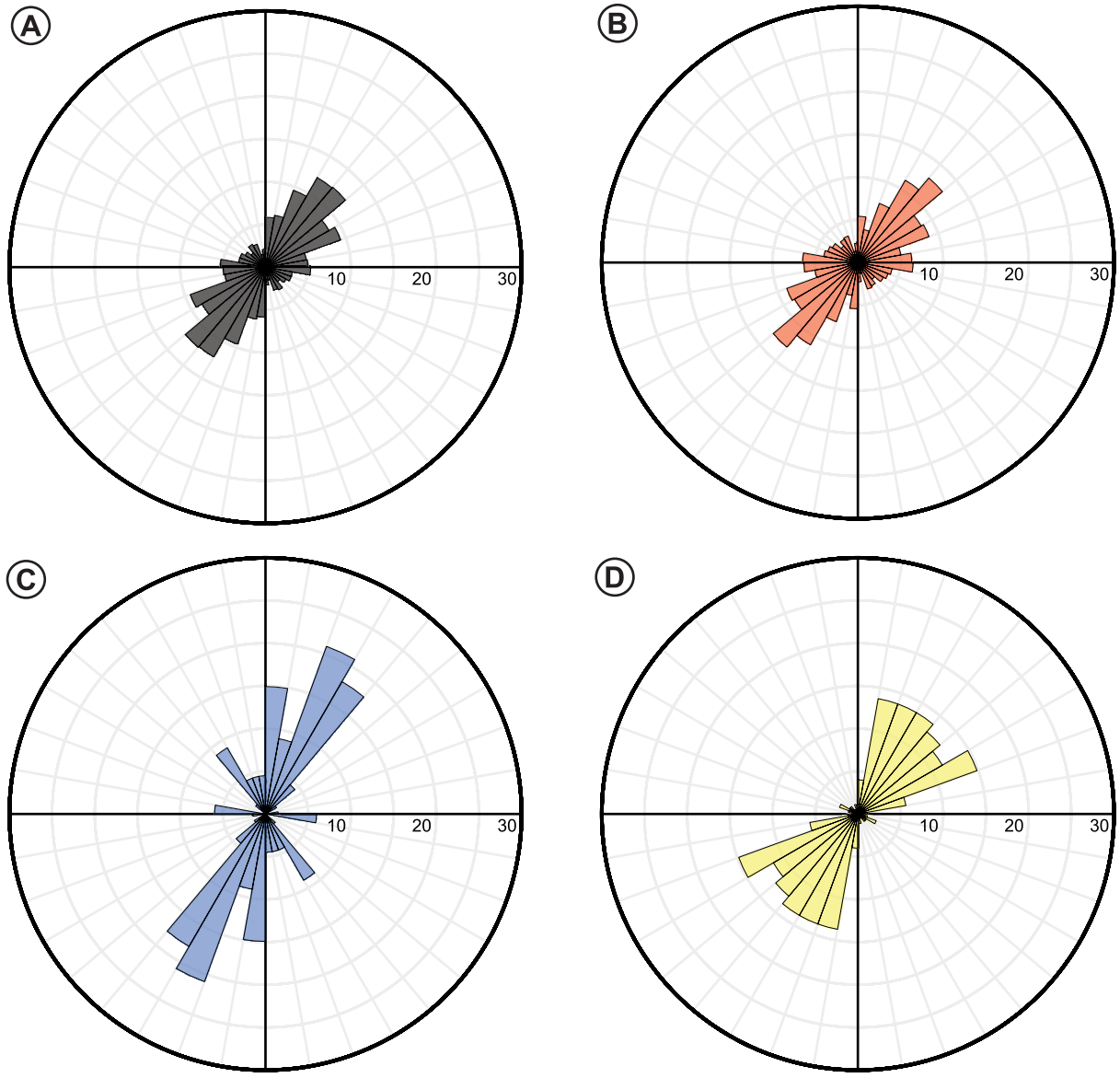

Figure 4. *Rose diagrams showing the orientation of lineaments determined by: A) All sources; B) DEM; C) Bathymetric data; D) Landsat imagery. Bin size = 10°.*

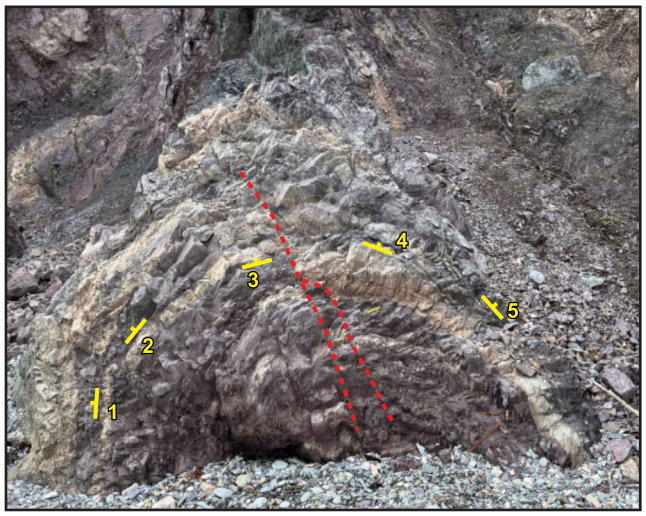

Plate 1. *Mesoscopic south-southwest-plunging asymmetric fold in interbedded purple shale and felsic tuff near the north end of the mafic tuff unit (Station 9). Note the steep southeastern limb and a gentler northwestern limb. Bedding at 1 (026°/87°), 2 (035°/65°), 3 (035°/48°), 4 (124°/15°), 5 (195°/56°) indicated in yellow; fault (217°/59°) indicated by red dashed line.*

near Station 12 (Figure 2C) locally appear to young to the southeast based on assumed normal grading. Farther to the northwest, moderately southeast-dipping sandstone beds contrast with shallowly west-dipping strata farther north (Figure 2D).

Folds

Mesoscopic folds are rare along the Bellevue Beach section. A plot of all poles to bedding measurements across the Bellevue section defines a girdle with a fold axis that plunges 19° toward 207° (Figure 5A). The asymmetric cylindrical fold at Station 9 has a steeply dipping southeastern limb and a gently dipping northwestern limb that intersect to define a fold axis that plunges 14° toward 205° (Figure 5B), based on five bedding measurements taken across the exposed fold surface (Plate 1). Additionally, an antiform characterizes the apparent hanging wall of the western fault at Station 12.

Cleavage

A regional penetrative cleavage developed in the stratiform sedimentary rocks dips moderately to steeply to the west, correlative with the regionally developed S_2 cleavage of Riveros (1998; Figure 5C). In the northern part of the section, the cleavage dips steeply to the east-southeast. A fracture cleavage is variably developed throughout the section. The bimodal lapilli tuff at Station 4 exhibits a foliation defined by flattened clasts having aspect ratios of up to 10:1 (average ~4:1) with a strike of 208° and a dip of 41°, consistent with the main regional S_m cleavage (designated S_2 by previous workers) in the sCB (Riveros, 1998) and Bonavista (Mills *et al.*, 2016a) areas.

Faults

A stereonet (Figure 6A) and rose diagram (Figure 6B) of all faults along the Bellevue section shows a south-southeast-striking group as the predominant trend. The other main groupings include east-southeast/west-northwest, northeast/southwest and a subset of S-striking faults. Detailed stereonet analyses (Figure 6C, D) were conducted at stations where conjugate fault geometries were observed.

At Station A, 137 m south-southeast of the drone section, southwest- and west-northwest- to east-southeast-strik-

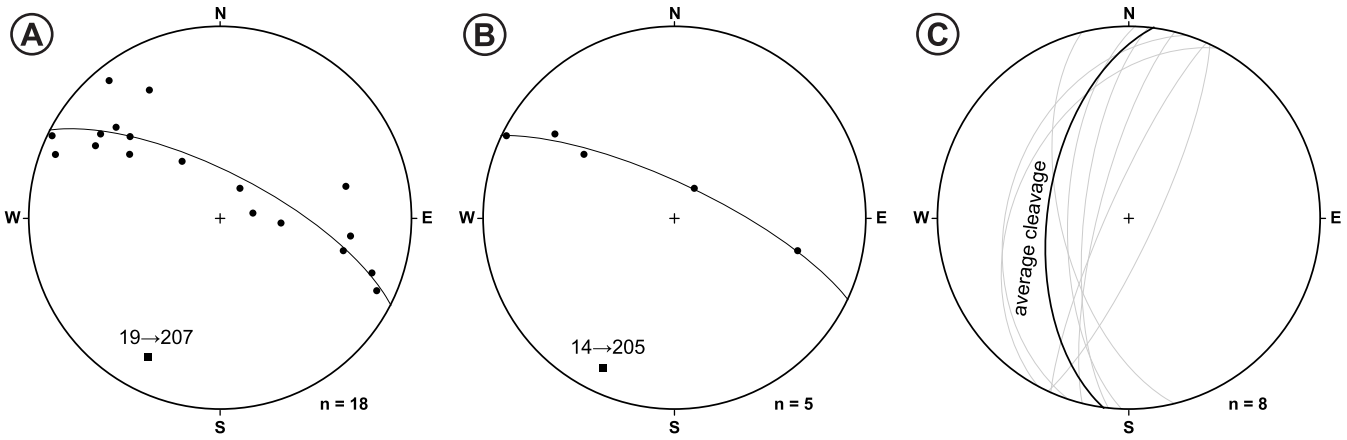

Figure 5. *Stereoplots of Bellevue Beach bedding and cleavage data. A) All bedding measurements plotted as poles to planes, defining a girdle with calculated fold axis of 19° plunging toward 207°; B) Bedding measurements define a girdle with a calculated fold axis of 14° plunging toward 205° for mesoscopic asymmetric anticline at Station 9; C) All cleavage measurements from the study area show an overall north-northeast trend.*

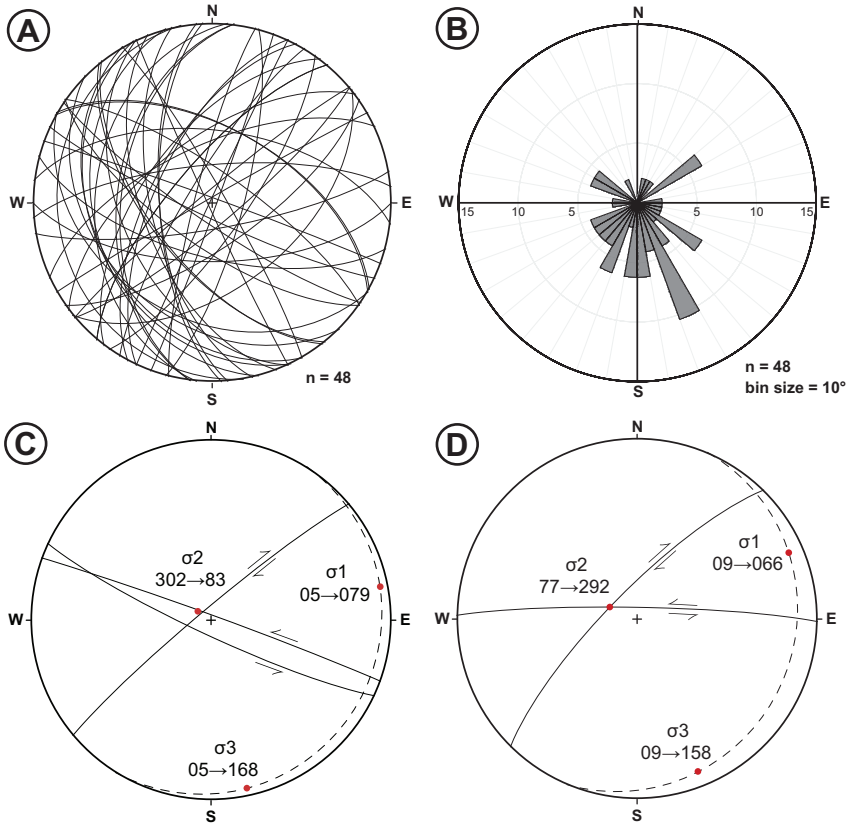

Figure 6. *Stereoplots for fault analyses across Bellevue Beach. A) All faults plotted as planes; B) Rose diagram showing the strike of faults along the Bellevue Beach section (bin size = 10°); C) west-northwest–east-southeast-striking and southwest-striking faults at Station A. The west-northwest-striking fault was used to calculate the principal stress components shown; D) West- and southwest-striking shear fractures at Station 6 form small horst and graben structures that indicate an average σ_1 of 09° toward 066°, subvertical σ_2 and σ_3 oriented at 09° toward 158°. (Note: dashed lines represent the motion planes.)*

ing faults present a geometry consistent with conjugate fault set development. Sinistral drag of cleavage is evident along the east-southeast-striking fault (Plate 2). The maximum compressional stress component (σ_1), which bisects the acute angle between the southwest- and west-northwest-striking faults, is calculated at 5° toward 079° (Figure 6C). Accordingly, the maximum extensional stress component (σ_3) is subhorizontal and north–south oriented, while the intermediate confining stress component (σ_2) is subvertical, compatible with a strike-slip deformational setting.

At Station 1, a moderately west-dipping fault is intersected by a steeply north-dipping fault. The latter fault crosscuts the former with dextral offset (Plate 3). This demonstrates that the steeply north-dipping fault postdates the moderately west-dipping fault. This example of a subvertical fault crosscutting a moderate or shallow fault recurs consistently across the Bellevue Beach area.

A shallowly west-dipping fault at Station 3 separates red rhyolite in the hanging wall from black rhyolite in the footwall. The structure is interpreted as a fault based on the erosional gap and pervasive buff-coloured alteration along the interface and patchy alteration in the apparent footwall (Plate 4). The sense of displacement is undetermined as no slickensides were observed.

At Station 6, small blocks displaying a horst and graben configuration are separated by shear fractures (Plate 5). One set is mainly southwest-striking (with minor northeast-striking fractures grouped in this set). The other set is west-striking. Both sets are steeply dipping. Stereonet analysis using the west-striking shear and the average orientation of the southwest- and northeast-striking shear fractures reflects a stress regime whereby the average principal stress components are: σ_1 (09° toward 066°), σ_2 (77° toward 292°) and σ_3 (09° toward 158°) (Figure 6D). The geometry of the shear fractures and their steep intermediate stress field component are consistent with a strike-slip setting.

An erosional incision into the coast-parallel section provides a rare cross-sectional perspective at Station 12 (Figure 7). The rock units at this station are subvertical and two subparallel faults cut the strata at a low angle relative to the primary layering. The western fault appears to contain a ramp anticline in its hanging wall, compatible with broadly east-directed thrusting. The orientation of the eastern fault (220°/80°) suggests that thrusting was approximately southeast-directed; the geometry of the imbricate thrusts here is consistent with northwest–southeast compression. A slightly overturned, tight to isoclinal fold occurs in the central, fault bounded block (Figure 7). It is unclear whether this tight folding and locally overturned bedding resulted from progressive deformation tied to a single compressional event or to a subsequent compressional event that tightened and steepened pre-existing structures.

Quartz Veins

Orientation data were collected for a small subset of the quartz veins observed at Bellevue Beach. Slightly sigmoidal, 1-cm-thick, quartz-filled tension gashes at Station 1

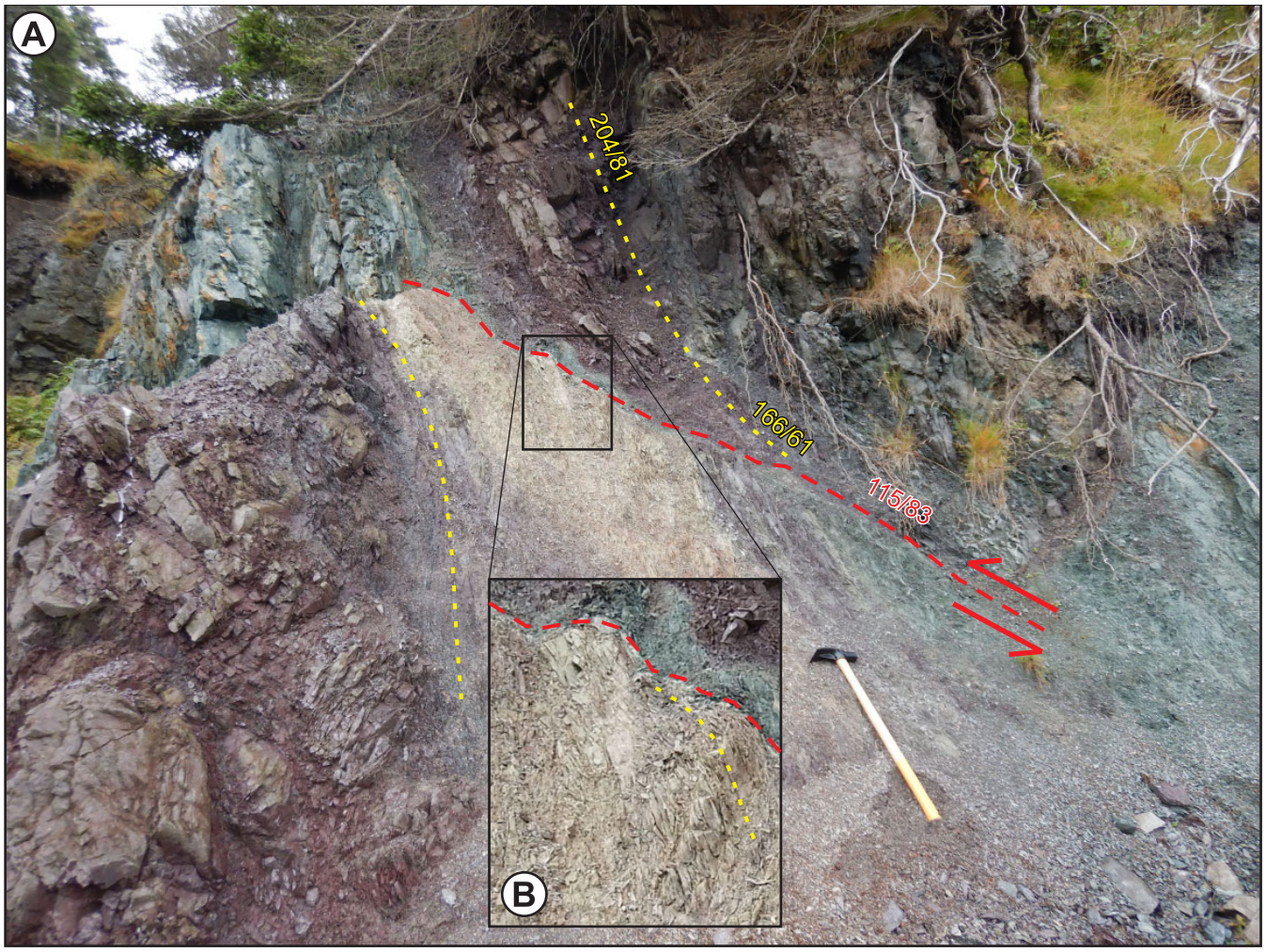

Plate 2. *Structural features present at Station A. A) Sinistral displacement with a small reverse component is indicated across a fault (red dashed line), as inferred by rotation of the cleavage (yellow dashed line) with proximity to the fault; B) Detail of cleavage rotation indicating sinistral drag.*

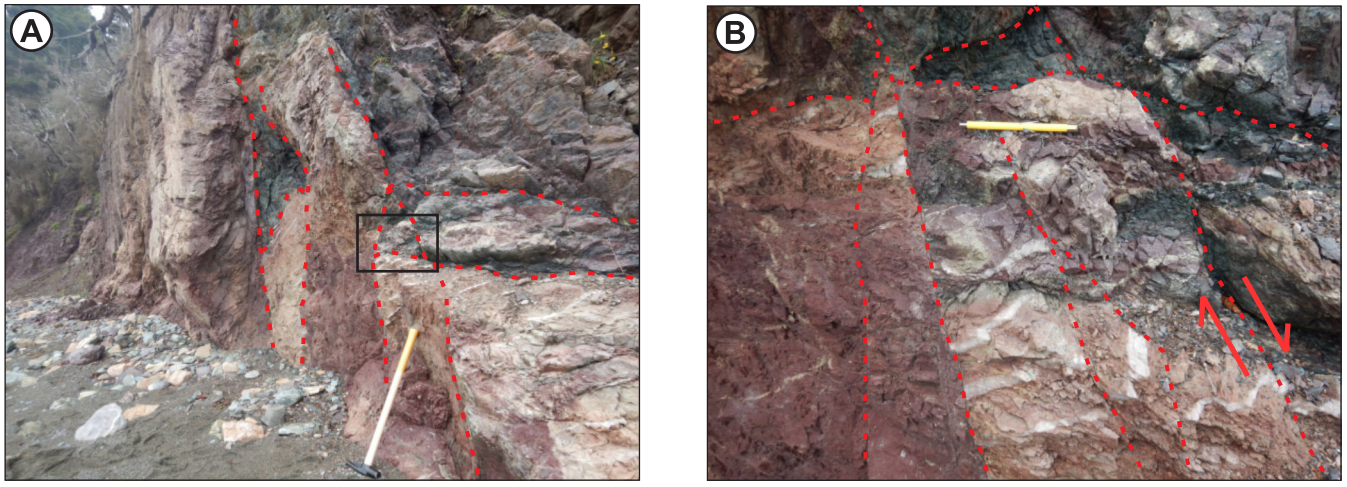

Plate 3. *A) A moderately west-dipping fault is crosscut and dextrally offset by a steeply north-dipping fault at Station 1; B) Detail from A showing quartz-filled tension gashes truncated by the steeply north-dipping fault.*

Plate 4. *Low-angle fault at Station 3 separating red rhyolite in the hangingwall from black rhyolite in the footwall.*

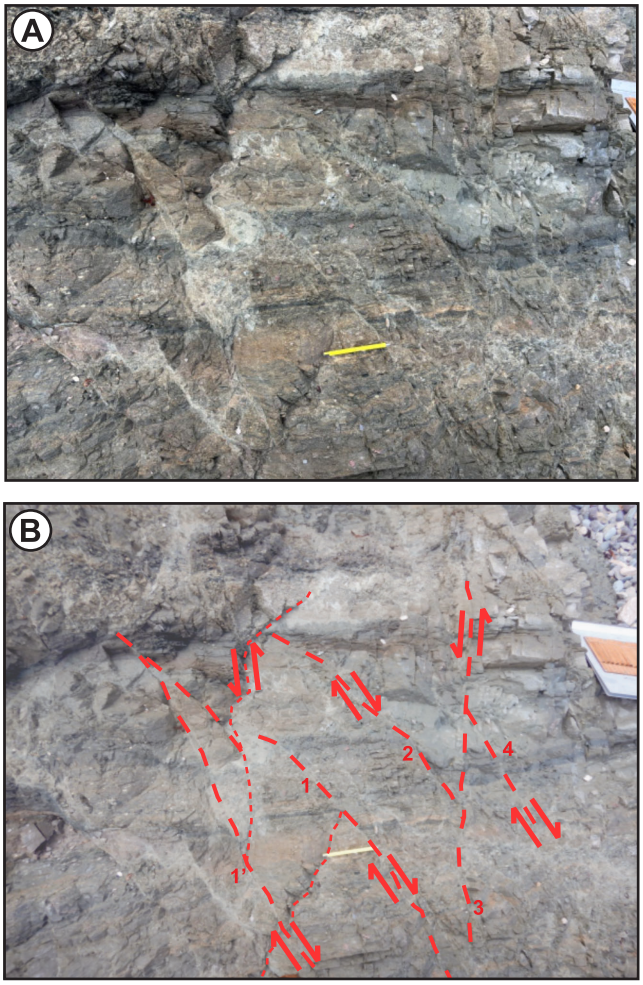

Plate 5. *A, B) Small horst and graben blocks at Station 6 separated by shear fractures (1 = 226°/70°; 2 = 209°/83°; 3 = 271°/85°; 4 = 046°/71°; 1' is subparallel to 1).*

dip shallowly to moderately to the south. Their length locally exceeds 20 cm, but averages about 10 cm and are commonly truncated by steeply north-dipping to vertical faults (Plate 3), clearly indicating that the steep faults postdate emplacement of the quartz veins. Centimetre-scale quartz veins at Station 8 display a slickenside that strikes 235° and dips 40° and has slickenlines that plunge 04° toward 246°, indicating strike-slip movement. A dm-scale, steeply north-dipping quartz vein at Station 14 is boudinaged and truncated by a subvertical northeast-trending fault. In all cases, the quartz veins are pre-tectonic relative to steep to vertical brittle faults.

DISCUSSION

INFERENCES FROM MAPPED FAULTS

Some of the lineaments in the study area coincide with faults on bedrock maps for the area (Figure 3; *e.g.*, Hutchinson, 1953; McCartney, 1967; King, 1988). Although the fault type for many of these is unknown, first-order kinematic inferences can be made based on the map pattern and available bedding orientations on existing bedrock maps. The mapped faults were examined to help link dominant lineament trends to inferred kinematic indicators.

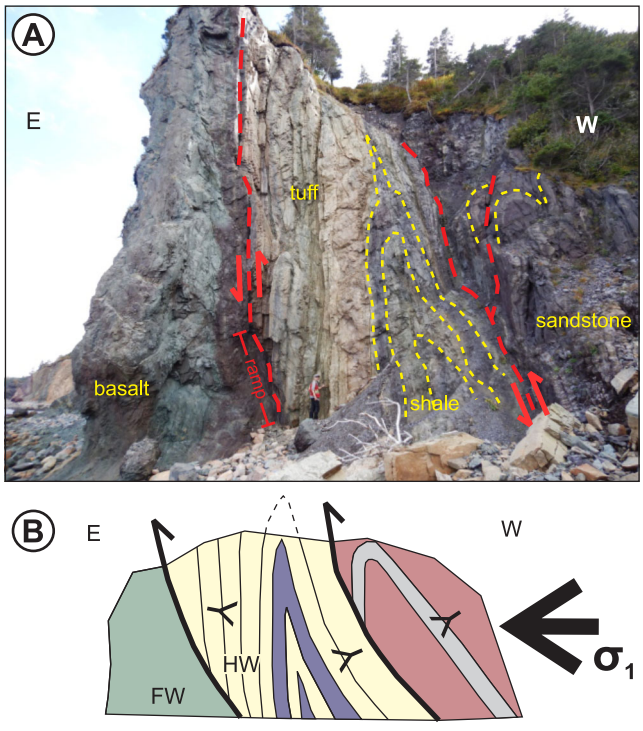

Figure 7. *A) Profile of subvertical faults at Station 12; B) Schematic cross-section for profile shown in A. The eastern fault has an orientation of 220°/80°. FW*–footwall, HW–hanging wall.

The east–west fault at Carbonear displays apparent sinistral offset of 1.1–1.5 km, based on the map pattern. Faults or lineaments of this orientation are relatively uncommon (<10% of identified lineaments by length; Table 2). Northwest-trending lineaments on the northern part of the isthmus are coincident with or parallel to the Jacks Pond Fault and Placentia Junction Fault and associated splays (Figure 3). The map pattern around the Jacks Pond Fault is suggestive of sinistral strike-slip movement, based on the displacement of the Connecting Point Group–Bull Arm Formation contact across the fault, whereas the sense of movement on the Placentia Junction Fault remains equivocal based on the lack of clearly displaced contacts across it. The north-trending Spread Eagle Thrust was interpreted by King (1988) as an east-directed thrust fault, and no discernable strike-slip component is evident based on the map pattern.

The northeast-trending Shearstown Brook Fault is subparallel to the Snows Pond syncline to the south and a syncline-anticline pair to the north (Figure 3). A northwest–southeast cross-section through the fault yields a profile geometry characterized by gently northwest-dipping beds in the northwest block and variable, but commonly subvertical bedding transitioning into an asymmetric syncline in the southeast block (Figure 8). Despite the lack of information on the orientation of the Shearstown Brook Fault, the profile geometry is consistent with a reverse (or thrust) fault interpretation whereby the northwest block occupies the hanging wall, and the steep beds and adjacent syncline on the southeast side are in the footwall. The contact between the upper St. John's and lower Signal Hill groups has either also been sinistrally displaced or truncated by the Shearstown Brook Fault. The latter case would require at least a slight overturning of the southeast limb of an asymmetric anticline in the hanging wall that was subparallel to the fault.

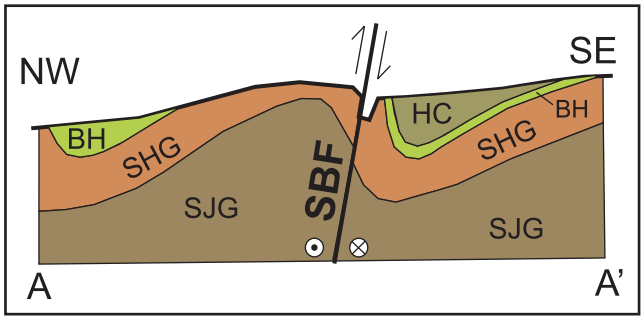

Figure 8. *Schematic cross-section through the Shearstown Brook Fault through line A-A' on Figure 3. BH–Big Head Formation, HC–Hearts Content Formation, SBF–Shearstown Brook Fault, SHG–Signal Hill Group (Gibbett Hill Formation), SJG–St. John's Group (Renews Head Formation).*

In the absence of age constraints on any of the faults described above, relative timing is explored below with the aim of proposing testable kinematic hypotheses. Rare fault offsets and truncation of both faults and quartz-filled tension gashes at Bellevue Beach suggest that multiple generations of faulting affected the area and the potential for fault reactivation is, therefore, high. Possible fault reactivation is particularly relevant to the Shearstown Brook Fault, particularly in consideration of the contrasting lineament patterns between the Bay de Verde Peninsula to the east and the isthmus areas to the west (Figure 3). Most lineaments on the east side of the Bay de Verde Peninsula trend east-northeast, or easterly around and just north of Carbonear. This dominant lineament trend transitions to more northeasterly toward the west side of the peninsula, particularly in the area between 5 to 10 km northeast of New Harbour. Similarly, a change in the dominant lineament trend is apparent in the Northwest Pond area and south of Long Harbour, where lineaments appear to transition from east-northeast-trending to more northeast- and north-northeast-trending in the area east of the Placentia Junction Fault and its easterly splay. North-trending lineaments are dominant in the southern isthmus area, between Chapel Arm and South Dildo (Figure 3), effectively dividing the study area into two domains: the Bay de Verde domain shows a counterclockwise transition of lineament orientations toward the west, and the northern isthmus domain shows a counterclockwise transition of lineament orientations toward the east. This pattern is consistent with progressive rotation of pre-existing lineament features with proximity to the southern part of the isthmus, where north-trending lineaments dominate. Both the Spread Eagle Thrust and the main trend apparent in the bathymetry data at southern Trinity Bay show a dominant north-trend. Taken together, the regional pattern is compatible with sinistral drag across the north-trending Spread Eagle Thrust or a parallel fault in its vicinity. This interpretation requires that lineaments in the Bay de Verde and isthmus blocks represent pre-existing structures that were progressively rotated in response to sinistral strike-slip motion along a principal shear zone broadly coincident with the Spread Eagle Thrust.

In this sinistral strike-slip scenario, the apparent rotation of the bedrock features reflected by the lineaments has implications for the interpretation of the Shearstown Brook Fault. If the southeast-directed thrust interpretation across the Shearstown Brook Fault is correct, then this fault is a pre-existing structure that must predate the inferred sinistral movement across the north-trending Spread Eagle Thrust. This interpretation also allows for a genetically linked origin for the northwest-trending lineaments prevalent in the New Harbour area and along the southwest coast of the Bay de Verde Peninsula. A small number of the lineaments derived from DEM and Landsat analysis, and most of those derived

from bathymetry in the New Harbour area, display a northwest (New Harbour) trend that dominates the coastline. They are typically 4–5 km in length and occur with a 1–2.5 km spacing over a 5 x 20 km, north-trending corridor along the southern Bay de Verde Peninsula. As they are prominent only within this narrow zone along the west side of the southern Bay de Verde Peninsula, they may reflect a structural origin that is distinct from other lineaments and faults in the region. Lineaments of the New Harbour trend have a consistent azimuth of 320°, which is oriented 50° counterclockwise from the 010° trend of the Spread Eagle Thrust and the parallel north-trending lineaments that dominate the southeastern part of the isthmus. If the origin of New Harbour lineaments is related to the north-trending Spread Eagle Thrust and its north-northeast-trending projection beneath Trinity Bay, then the relatively high angle between the two trends suggests that the short northwest-trending features likely developed antithetic to the principal shear zone, inferred to be subparallel to the Spread Eagle Thrust. Accordingly, these structures may be interpreted as R shears or T fractures (*e.g.*, Ahlgren, 2001; Davis *et al.*, 2000).

STRUCTURAL SYNTHESIS

Early Compression (D_1 Elements)

Parallel thrust faults at Bellevue Beach (Station 12; Figures 2C and 7) are consistent with southeast-directed thrust imbrication, similar to that documented in the Brigus area of sCB (Riveros, 1998). Because the thrusts are oriented at a low angle to primary layering, they likely originated as low-angle structures. The current subvertical arrangement of the faults and layering, and the associated tight fold in the central block (Figure 7), are interpreted to result from subsequent east–west compression during the main regional compressional event, D_m (or D_2 of Riveros, 1998 and Mills *et al.*, 2016a), which steepened and tightened pre-existing faults and associated folds. The low-angle thrust faults are therefore considered elements of an early, D_1, event, possibly related to the late Ediacaran Avalonian orogeny (Anderson *et al.*, 1975; Lowe *et al.*, 2022; Beranek *et al.*, 2023; Serna Ortiz and Lowe, 2024). Some of the northeast-trending lineaments in the isthmus area, particularly the Shearstown Brook Fault, are also interpreted as early (D_1) structures produced during Avalonian deformation, consistent with southeast-directed thrust imbrication interpreted for northeast-trending (southwest-striking) Precambrian thrust faults in the sCB area (Riveros, 1998). Because the Shearstown Brook Fault apparently does not crosscut upper Precambrian units above the Gibbett Hill Formation (Signal Hill Group; Figure 3), it may have formed prior to deposition of these upper Precambrian units or alternatively developed as a blind fault that was not exposed during latest Precambrian sedimentation. Similar blind thrusts and syndeformational sedimentation related to Avalon orogenesis are proposed on the eastern Avalon Peninsula (Serna Ortiz and Lowe, 2024).

Early Sinistral (D_2 Elements)

A north-trending principal shear zone, parallel to King's (1988) Spread Eagle Thrust and extending northwards beneath Trinity Bay, is proposed to separate lineament rotational trends in the Bay de Verde domain from those observed in the isthmus domain. The former shows a westward progressive counterclockwise rotation of lineaments whereas the latter shows an eastward progression of counterclockwise rotation. The rotation of structural elements on opposite sides of this fault is compatible with sinistral movement across a north-trending principal shear zone that is located between Chapel Arm and South Dildo, likely near and parallel to the Spread Eagle Thrust. Such rotation necessitates that the rotated structural elements are pre-existing (D_1) structures, with their rotation linked to a later, D_2, sinistral event. Because some of the lineaments interpreted to have participated in this rotation crosscut Cambrian units, the sinistral displacement event is interpreted to be post-Cambrian. This sinistral event allows the elegant and testable corollary that the short, northwest-trending lineaments of the New Harbour trend represent extensional R or T shears that formed coeval with and antithetic to post-Cambrian sinistral movements. Evidence of this sinistral event in the current study area derives exclusively from the lineament analysis.

Juxtaposition of two distinct Ediacaran basins on the Bonavista Peninsula is attributed to oblique sinistral transpression recorded as north-directed thrust imbrication along the south side of the peninsula and coeval sinistral movement on the east side of the peninsula (Mills *et al.*, 2024). Sinistral strike-slip deformation in central Avalon Zone may be related to the sinistral-oblique accretion of Avalonia to composite Laurentian at *ca.* 422–394 Ma (Caron, 1994; Holdsworth, 1994; D'Lemos *et al.*, 1997; Kellett *et al.*, 2016). This event is interpreted to precede the east–west compression linked to the regional, post-Cambrian north-northeast- and south-southwest-folds and associated axial planar penetrative cleavage (S_m) because this scenario is consistent with kinematic constraints on the Dover Fault, where sinistral movements demonstrably precede dextral movements and fault reactivation (Caron, 1994; Holdsworth, 1994; D'Lemos *et al.*, 1997; Kellett *et al.*, 2016). Accordingly, the sinistral deformation on the Isthmus is assigned to D_2, whereas the main cleavage, formerly assigned to D_2 by Riveros (1998) and Mills *et al.* (2016a), is reassigned here to a subsequent deformation phase (D_3).

Regional East–West Compression (D_3 Elements)

The main cleavage (S_m) shows some variation (Figure 5C) but is generally steeply dipping and south-southwest-striking and is approximately axial planar to meso- and macroscopic folds developed in the Bellevue Beach area. North- to north-northeast-trending axial planes and cleavage affect Cambrian units and, in eastern Avalon Zone, have traditionally been attributed to regional, east–west compression related to Avalonian accretion (*e.g.*, Anderson, 1975; Riveros, 1998), commonly designated as D_2 (*e.g.*, Riveros, 1998; Mills *et al.*, 2016a). However, the regionally developed penetrative cleavage may instead be linked to subsequent (post-sinistral D_2) deformation associated with dextral fault zones showing limited lateral displacement but commonly reactivating sinistral fault zones in the northwestern Avalon Zone. In this region, these faults postdate Avalonian docking but likely formed by *ca.* 385 Ma (Kellett *et al.*, 2016). Alternatively, regional east–west compression (or transpression) may be linked to still later Carboniferous deformation related to the assembly of Pangea (*e.g.*, Stampfli *et al.*, 2013; Waldron *et al.*, 2015). Whether related to post-Avalonia docking processes, such as accretion of the Meguma terrane (Culshaw and Liesa, 2011; Waldron *et al.*, 2015) or to Pangean assembly, development of the regional S_m cleavage is incompatible with sinistral, D_2, deformation and is more compatible with east–west shortening during a subsequent, regional D_3 event.

The shallowly south-dipping tension gashes at Station 1 reflect a stress regime characterized by an east–west maximum compressive stress and north–south oriented maximum extension. Their geometry and stress regime are therefore compatible with regional D_3 deformation but were likely developed during a slightly later unroofing event, in keeping with their inferred extensional origin. Such extension following the main D_{3a} compression, might be considered a linked event (D_{3b}).

Late Conjugate Brittle Faults (D_4)

Truncation of D_{3b} tension gashes by a set of conjugate north- and east-northeast-trending faults implies that a brittle event post-dates D_{3b}. These conjugate faults developed under a stress regime having a northeasterly σ_1, a southeasterly σ_3 and a subvertical σ_2 (Figure 6C, D), consistent with strike-slip deformation. Without clear evidence on the sense of displacement, the stress regime is compatible with either northeast–southwest transpression or northwest–southeast extension, possibly linked to either Pangea amalgamation or breakup, respectively (*e.g.*, Welford, 2024; Willner *et al.*, 2015).

FUTURE RESEARCH

Further detailed structural investigations are recommended for the Bellevue Beach area. This work would be complemented by lithogeochemical studies, particularly to develop a chemostratigraphic framework for the volcanic rocks that dominate the section, as well as to better constrain the original tectonic setting for these rocks. An improved stratigraphic framework could help to constrain the sense and magnitude of displacement on at least some of the faults in the area. Although dating of brittle faulting is notoriously challenging, fault breccias elsewhere have been successfully dated radiometrically, by $^{40}Ar/^{39}Ar$ geochronology on whole-rock, white mica and K-feldspar, to constrain multiple fault reactivation episodes (Eide *et al.*, 1997; Kellett *et al.*, 2016, 2024). The potential for achieving erroneous results from radiometric dating owing to the inherent mixture of detrital and authigenic phyllosilicates in a fault breccia, and to loss of ^{39}Ar during irradiation, can be greatly reduced by combining Ar analysis with X-ray analysis to constrain the ratio of authigenic to detrital material (*e.g.*, van der Pluijm *et al.*, 2001).

If the level of outcrop exposure permits, a detailed structural investigation in the vicinity of the Spread Eagle Thrust (King, 1988) is recommended to constrain the sense and possibly the magnitude of displacement across this regionally important fault. Although no lateral displacement is evident from the map pattern, the lineament pattern is compatible with sinistral strike-slip motion across either the Spread Eagle Thrust (or a nearby parallel fault zone), producing the apparent rotation of structural elements into near-parallelism with proximity to the Spread Eagle Thrust. A local detailed study could test the veracity of this proposal. In addition, a structural investigation along the western margin of the southern Bay de Verde Peninsula is recommended to test whether the southwest lineaments there might represent extensional R or T shears.

Sedimentological, stratigraphic and provenance studies (*e.g.*, detrital zircon geochronology) on previously correlated upper Ediacaran units (*e.g.*, Big Head, Maturin Ponds and Hearts Content formations; King, 1988) in both the isthmus and Bay de Verde areas are recommended to address the apparent age discrepancy between these successions. The contrast in ages of rocks assigned to the Big Head Formation on the isthmus and on the Bay de Verde Peninsula (King, 1988) has been noted previously (Mills and Álvaro, 2023). Rocks assigned to the Big Head Formation on the isthmus block near Long Harbour contain a distinctive diamictite unit that may be correlative (Brückner, 1977; Mills and Sandeman, 2021) to the *ca.* 580 Ma Gaskiers Formation and Trinity diamictite (Pu *et al.*, 2016; Gómez *et al.*, 2025) on

Avalon and Bonavista peninsulas, respectively. Rocks assigned to the Big Head Formation on the Bay de Verde Peninsula, however, conformably overlie the *ca.* 565 Ma Mistaken Point Formation (Matthews *et al.*, 2020) and *ca.* 562 Ma St. John's Group (Canfield *et al.*, 2020). This stratigraphic discrepancy also highlights the potential importance of the Spread Eagle Thrust as a long-lived, possibly reactivated, crustal-scale structure.

ACKNOWLEDGMENTS

Heather Campbell and Jennifer Organ provided valuable insight into the identification of surficial landforms in the area, allowing for the exclusion of these features from the lineament data set and analysis. We extend thanks to Ian Honsberger and Alana Hinchey for their thoughtful reviews of this manuscript.

REFERENCES

Ahlgren, S.G.
2001: The nucleation and evolution of Riedel shear zones as deformation bands in porous sandstone. Journal of Structural Geology, Volume 23, pages 1203-1214.

Ahmadi, H. and Pekkan, E.
2021: Fault-based geological lineaments extraction using remote sensing and GIS–a review. Geosciences, Volume 11.
https://doi.org/10.3390/geosciences11050183

Allmendinger, R.W., Cardozo, N.C. and Fisher, D.
2013: Structural Geology Algorithms: Vectors & Tensors. Cambridge, England, Cambridge University Press, 289 pages.

Anderson, M.M., Brückner, W.D., King, A.F. and Maher, J.B.
1975: The late Proterozoic "H.D. Lilly Unconformity" at Red Head, northeastern Avalon Peninsula, Newfoundland. American Journal of Science, Volume 275, pages 1012-1027.

Beranek, L.P., Hutter, A.D., Pearcey, S., James, C., Langor, V., Pike, C., Goudie, D. and Oldham, L.
2023: New evidence for the Baltican cratonic affinity and Tonian to Ediacaran tectonic evolution of West Avalonia in the Avalon Peninsula, Newfoundland, Canada. Precambrian Research, Volume 390, pages 1-19. https://doi.org/10.1016/j.precamres.2023.107046

Bilmes, A., D'Elia, L., Lopez, L., Richiano, S., Varela, A., Alvarez, M., Bucher, J., Eymard, I., Muravchik, M., Franzese, J. and Ariztegui, D.
2019: Digital outcrop modelling using "structure-from-motion" photogrammetry: Acquisition strategies, validation and interpretations to different sedimentary environments. Journal of South American Earth Sciences, Volume 96.
https://doi.org/10.1016/j.jsames.2019.102325

Blackwood, R.F. and Kennedy, M.J.
1975: The Dover Fault: western boundary of the Avalon Zone in northeastern Newfoundland. Canadian Journal of Earth Sciences, Volume 12, pages 320-325.

Brückner, D.
1977: Significance of new tillite finds for east-west correlation of Proterozoic Avalon-zone formations in southeastern Newfoundland (Canada). Estudios Geológicos, Volume 33, pages 95-102.

Calon, R.A.
2017: Structure and evolution of the Flat Rock thrust zone in the Torbay Area, eastern Avalon Zone, Appalachians of Newfoundland. Unpublished B.Sc. (Hons) thesis. Memorial University of Newfoundland, St. John's, Newfoundland and Labrador, 131 pages.

Calon, T.
2001: Late Precambrian sedimentation and related orogenesis of the Avalon Peninsula, eastern Avalon Zone, Newfoundland. Geological Association of Canada, St. John's 2001 Field Trip Guidebook, A9/B8, pages 1-32.

Canfield, D.E., Knoll, A.H., Poulton, S.W., Narbonne, G.M. and Dunning, G.R.
2020: Carbon isotopes in clastic rocks and the Neoproterozoic carbon cycle. American Journal of Science, Volume 320, pages 97-124.
https://doi.org/10.2475/02.2020.01

Caron, A.
1994: Structural and microstructural study of the Dover Fault and its country rocks: an example of a reactivated transpressional zone in northeastern Newfoundland. Unpublished Ph.D. thesis. University of New Brunswick, Fredericton, New Brunswick, 367 pages.

Chesley, J.T., Leier, A.L., White, S. and Torres, R.
2017: Using unmanned aerial vehicles and structure-from-motion photogrammetry to characterize sedimentary outcrops: An example from the Morrison Formation, Utah, USA. Sedimentary Geology, Volume

354, pages 1-8.
http://dx.doi.org/10.1016/j.sedgeo.2017.03.013

Culshaw, N. and Liesa, M.
2011: Alleghanian reactivation of the Acadian fold belt, Meguma Zone, southwest Nova Scotia. Canadian Journal of Earth Sciences, Volume 34, pages 833-847.

Davis, G.H., Bump, A.P., García, P.E. and Ahlgren, S.G.
2000: Conjugate Riedel deformation band shear zones. Journal of Structural Geology, Volume 22, pages 169-190.

D'Lemos, R.S., Schofield, D.J., Holdsworth, R.E. and King, T.R.
1997: Deep crustal and local rheological controls on the siting and reactivation of fault and shear zones, north-eastern Newfoundland. Journal of the Geological Society, Volume 154, pages 117-121.

Eide, E.A., Torsvik, T.H. and Andersen, T.B.
1997: Absolute dating of brittle fault movements: Late Permian and Late Jurassic extensional fault breccias in western Norway. Terra Nova, Volume 9, pages 135-139.

Fitzgerald, D.M., Narbonne, G.M., Pufahl, P.K. and Dalrymple, R.W.
2024. The Mall Bay Formation (Ediacaran) and the protracted onset of the Gaskiers glaciation in Newfoundland, Canada. Precambrian Research, Volume 405.
https://doi.org/10.1016/j.precamres.2024.107369

Gómez, N., Lowe, D., Mills, A., Kommescher, S. and Lam, R.
2025: Interplay of Ediacaran glaciation and sediment provenance revealed by detrital zircon U–Pb geochronology and Hf isotope geochemistry in the Bonavista Peninsula (Newfoundland). Geological Society of America. https://doi.org/10.1130/B38347.1

Hayes, A.O.
1948: Geology of the area between Bonavista and Trinity bays, eastern Newfoundland. Geological Survey of Newfoundland, Bulletin 32 (Part 1), pages 1-37.

Holdsworth, R.E.
1994: Structural evolution of the Gander–Avalon terrane boundary: A reactivated transpression zone in the NE Newfoundland Appalachians. Journal of the Geological Society of London, Volume 151, pages 629-646.

Howse, A.F. and Maloney, J.
1984: Barite deposits of the Avalon Peninsula. *In* Mineral Deposits of Newfoundland – A 1984 perspective. *Edited by* M.J. Murray. Government of Newfoundland and Labrador, Department of Mines and Energy, Mineral Development Division, Report 84-03, pages 173-177.

Hutchinson, R.D.
1953: Geology of Harbour Grace map-area, Newfoundland. Geological Survey of Canada, Memoir 275, 43 pages.

Jackisch, R., Lorenz, S., Kirsch, M., Zimmermann, R., Tusa, L., Pirttijärvi, M., Saartenoja, A., Ugalde, H., Madriz, Y., Savolaines, M. and Gloaugen, R.
2020: Integrated geological and geophysical mapping of a carbonatite-hosting outcrop in Siilinjärvi, Finland, using unmanned aerial systems. Remote Sensing, Volume 12. https://doi.org/10.3390/rs12182998

Jenness, S.E
1963: Terra Nova and Bonavista map-areas, Newfoundland (2D E ½ and 2C). Geological Survey of Canada, Memoir 327, 184 pages.

Kellett, D.A., Larson, K.P. and Skipton, D.R.
2024: Integration of white mica *in situ* $^{87}Rb/^{87}Sr$ with in situ and step-heat $^{40}Ar/^{39}Ar$ dates in orogenic settings. Lithos, Volume 482.
https://doi.org/10.1016/j.lithos.2024.107687

Kellett, D.A., Warren, C., Larson, K.P., Zwingmann, H., van Staal, C.R. and Rogers, N.
2016: Influence of deformation and fluids on Ar retention in white mica: Dating the Dover Fault, Newfoundland Appalachians. Lithos, Volume 254-255, pages 1-17. https://doi.org/10.1016/j.lithos.2016.03.003

King, A.F.
1988: Geology of the Avalon Peninsula, Newfoundland (parts of 1K, 1L, 1M, 1N and 2C). Government of Newfoundland and Labrador, Department of Mines, Mineral Development Division, Map 88-01.

Lazzari, M. and Gioia, D.
2017: UAV images and historical aerial-photos for geomorphological analysis and hillslope evolution of the Uggiano medieval archeological site (Basilicata, southern Italy). Geomatics, Natural Hazards and Risk, Volume 8, Number 1, pages 104-119.
https://doi.org/10.1080/19475705.2017.1310762

Lowe, D.G., Serna Ortiz, S., Mills, A., Stanley, B.F. and Khatrine, G.
2022: The Signal Hill Group, Newfoundland, Canada: A record of pre-vegetated fluvio-deltaic response to

progressive Neoproterozoic deformation during the Avalonian Orogeny. Atlantic Geoscience Society, 48th Colloquium and Annual General Meeting 2022, Program and Abstracts, Volume 58, pages 21-22.

Malpas, J.G.
1971: The petrochemistry of the Bull Arm Formation near Rantem Station, southeast Newfoundland. Unpublished M.Sc. thesis. Memorial University of Newfoundland, St. John's, NL, 122 pages.

Matthews, J.J., Liu, A.G., Yang, C., McIlroy, D., Levell, B. and Condon, D.J.
2020: A chronostratigraphic framework for the rise of the Ediacaran macrobiota: New constraints from Mistaken Point Ecological Reserve, Newfoundland. Geological Society of America, Bulletin 133, Number 34, pages 612-624.

McCartney, W.D.
1957: Dildo, Avalon Peninsula, Newfoundland. Geological Survey of Canada, Preliminary Map 13-1956.

1958: Sunnyside, Island of Newfoundland. Geological Survey of Canada, Preliminary Map 18-1958.

1967: Whitbourne map Area, Newfoundland. Geological Survey of Canada, Memoir 341, 135 pages.

McHenry, M. and Dunlop, P.
2016: The subglacial imprint of the last Newfoundland Ice Sheet, Canada. Journal of Maps, Volume 12, Number 3, pages 462-483.
https://doi.org/10.1080/17445647.2015.1044038

Menegoni, N., Meisina, C., Perotti, C. and Crozi, M.
2018: Analysis by UAV digital photogrammetry of folds and related fractures in the Monte Antola Flysch Formation (Ponte Organasco, Italy). Geosciences, Volume 8. https://doi.org/10.3390

Miller, H.G. and Singh, V.
1995: The Avalon Terrane of Newfoundland: geophysical correlations from onshore to offshore as evidence for Precambrian structural evolution. Tectonophysics, Volume 242, pages 183-197.

Mills, A.J.
2014: Preliminary results from bedrock mapping in the Sweet Bay area (parts of NTS map areas 2C/5 and 2C/12), western Bonavista Peninsula, Newfoundland. *In* Current Research. Government of Newfoundland and Labrador, Department of Natural Resources, Geological Survey, Report 14-1, pages 135-154.

Mills, A.J. and Álvaro, J.J.
2023: Lithogeochemical features of Cambrian basalts from the western Avalon Peninsula, Avalon Terrane, Newfoundland: Alkaline magmatism along an inherited fault zone. *In* Current Research. Government of Newfoundland and Labrador, Department of Industry, Energy and Technology, Geological Survey, Report 23-1, pages 197-220.

Mills, A.J., Calon, T. and Peddle, C.
2016a: Preliminary investigations into the structural geology of the Bonavista Peninsula, northeast Newfoundland. *In* Current Research. Government of Newfoundland and Labrador, Department of Natural Resources, Geological Survey, Report 16-1, pages 133-152.

Mills, A.J., Dunning, G.R. and Langille, A.
2016b: New geochronological constraints on the Connecting Point Group, Bonavista Peninsula, Avalon Zone, Newfoundland. *In* Current Research. Government of Newfoundland and Labrador, Department of Natural Resources, Geological Survey, Report 16-1, pages 153-171.

Mills, A.J., Dunning, G.R., Murphy, M. and Langille, A.
2017: New geochronological constraints on the timing of magmatism for the Bull Arm Formation, Musgravetown Group, Avalon Terrane, Newfoundland. *In* Current Research. Government of Newfoundland and Labrador, Department of Natural Resources, Geological Survey, Report 17-1, pages 1-17.

Mills, A. and Jones, V.
2024: New structural observations on the southern Burin Peninsula, Avalon Zone, Newfoundland. *In* Current Research. Government of Newfoundland and Labrador, Department of Industry, Energy and Technology, Geological Survey, Report 24-1, pages 181-204.

Mills, A.J., Normore, L., Gomez, N., Dunning, G.R. and Lowe, D.G.
2024: A tale of two basins: Juxtaposition of the Ediacaran fossil-bearing St. John's Basin against the Ediacaran glaciovolcanic Bonavista Basin on the Bonavista Peninsula, Avalon Zone, Newfoundland. Atlantic Geoscience, Volume 60, pages 131-150.
https://doi.org/10.4138/atlgeo.2024.007

Mills, A.J. and Sandeman, H.A.I.
2021: Reconnaissance lithogeochemical investigation of the Bull Arm Formation and significance of diamictite in the overlying Big Head Formation in the Long Harbour–Placentia area, western Avalon Peninsula, Newfoundland. *In* Current Research. Government of Newfoundland and Labrador, Department of Industry, Energy and Technology, Geological Survey, Report 21-1, pages 73-96.

Mills, J.E.
1991: The geology and volcanic evolution of the Bull Arm Formation – Isthmus of Avalon. Unpublished B.Sc. (Hons) thesis. Memorial University of Newfoundland, St. John's, Newfoundland, 92 pages.

Myrow, P.M.
1995: Neoproterozoic rocks of the Newfoundland Avalon Zone. Precambrian Research, Volume 73, pages 123-136.

Norris, S.L., Organ, J., Dyke, A.S., Neligan, T., Stanton, C.C., Strickland, K. and Gosse, J.C.
2024: Glacial geomorphology of Newfoundland, Canada. Journal of Maps, Volume 20, Number 1, Article 2386296.
https://doi.org/10.1080/17445647.2024.2386296

Peace, A.L. and Jess, S.
2022: Microdrones in field-based structural geology: A photogrammetry and fracture quantification case study from the North Mountain Basalt, Nova Scotia, Canada. Drone Systems and Applications, Volume 11, pages 1-15. https://dx.doi.org/10.1139/dsa-2022-0037

Peddle, C.
2017: Structural analysis of the Country Pond anticline and Bay Bulls syncline pair, eastern Avalon Zone, Newfoundland. Unpublished B.Sc. thesis. Memorial University of Newfoundland, St. John's, Newfoundland and Labrador, 101 pages.

Pu, J.P., Bowring, S.A., Ramezani, J., Myrow, P., Raub, T.D., Landing, E., Mills, A., Hodgin, E. and Macdonald, F.A.
2016: Dodging snowballs: Geochronology of the Gaskiers glaciation and the first appearance of the Ediacaran biota. Geology, Volume 44, pages 955-958. https://doi.org/10.1130/G38284.1

Rice, T.G.
1996: Structure of the Flat Rock thrust zone, Avalon Peninsula, Newfoundland Appalachians. Unpublished B.Sc. (Hons) thesis. Memorial University of Newfoundland, St. John's, Newfoundland, 117 pages.

Riveros, C.
1998: Structural geology of the southwestern shore of Conception Bay, Eastern Avalon Zone, Newfoundland Appalachians. Unpublished M.Sc. thesis. Memorial University of Newfoundland, St. John's, Newfoundland.

Serna Ortiz, S. and Lowe, D.G.
2024: Stratal evolution and provenance of a Precambrian delta in a tectonically active terrane: The lower Signal Hill Group, Avalon Zone, Newfoundland. Precambrian Research, Volume 401.
https://doi.org/10.1016/j.precamres.2023.107274

Stampfli, G.M., Hochard, C., Vérard, C. and Wilhem, C.
2013: The formation of Pangea. Tectonophysics, Volume 593, pages 1-19.

Van der Pluijm, B.A., Hall, C.M., Vrolijk, P.J., Pevear, D.R. and Covey, M.C.
2001: The dating of shallow faults in the Earth's crust. Nature, Volume 412, pages 172-175.

Waldron, J.W.F., Barr, S.M., Park, A.F., White, C.E. and Hibbard, J.P.
2015: Late Paleozoic strike-slip faults in Maritime Canada and their role in the reconfiguration of the northern Appalachian orogen. Tectonics, Volume 34, pages 1661-1684.
https://doi.org/10.1002/2015TC003882

Waldron, J.W.F., McCausland, P.J., Barr, S.M., Schofield, D.I., Reusch, D. and Wu, L.
2022: Terrane history of the Iapetus Ocean as preserved in the northern Appalachians and western Caledonides. Earth-Science Reviews, Volume 233, pages 104-163.

Welford, K.
2024: Crustal structure of onshore-offshore Atlantic Canada and environs from constrained 3-D gravity inversion using variable mesh depths. Geophysical Journal International, Volume 236, pages 798-818. https://doi.org/10.1093/gji/ggad448

Wilner, A.P., Barr, S.M., Glodny, J., Massonne, S., Thompson, S.N., van Staal, C.R. and White, C.E.
2015: Effects of fluid flow, cooling and deformation as recorded by $^{40}Ar/^{39}Ar$, Rb-Sr and zircon fission track ages in very low- to low-grade metamorphic rocks in Avalonian SE Cape Breton Island (Nova Scotia, Canada). Geological Magazine, Volume 152, pages 767-787.